Water Resources Research

RESEARCH ARTICLE
10.1029/2023WR034454

Explaining the Statistical Properties of Salt Intrusion in Estuaries Using a Stochastic Dynamical Modeling Approach

Henk A. Dijkstra[1], Bouke Biemond[1], Jiyong Lee[1], and Huib E. de Swart[1]

[1]Institute for Marine and Atmospheric Research Utrecht, Utrecht University, Utrecht, The Netherlands

Key Points:

- A stochastic dynamical model is developed to explain the statistics of salt intrusion in estuaries
- Additive (multiplicative) noise in river discharge induces a positive (negative) skewness in the salt intrusion length statistics
- Both additive and multiplicative noise in river discharge are important forthe salt intrusion statistics in the San Francisco Bay estuary

Correspondence to:
H. A. Dijkstra,
h.a.dijkstra@uu.nl

Citation:
Dijkstra, H. A., Biemond, B., Lee, J., & de Swart, H. E. (2023). Explaining the statistical properties of salt intrusion in estuaries using a stochastic dynamical modeling approach. *Water Resources Research*, *59*, e2023WR034454. https://doi.org/10.1029/2023WR034454

Received 13 JAN 2023
Accepted 9 JUL 2023

Abstract Determining the statistical properties of salt intrusion in estuaries on sub-tidal time scales is a substantial challenge in environmental modeling. To study these properties, we here extend an idealized deterministic salt intrusion model to a stochastic one by including a stochastic model of the river discharge. In the river discharge model, two types of stochastic forcing are used: one independent (additive noise) and one dependent (multiplicative noise) on the river discharge state. Each type of forcing results in a non-Gaussian response in the salt intrusion length, which we consider here as the distance of the 2 psu isohaline contour to the estuary mouth. The salt intrusion model including both types of stochastic forcing in the river discharge provides a satisfactory explanation of the multi-year statistics of observed salt intrusion lengths in the San Francisco Bay estuary, in particular for the skewness of its probability density function.

1. Introduction

With increasing probability of dry periods in a warming climate, salt intrusion in estuaries is becoming an urgent problem in many coastal areas (Eslami et al., 2021). Salt intrusion is influenced by many processes which show variability on a wide range of time scales. On hourly scales, variations in wind velocity (or direction) and tidal water level are significant. On daily scales, river discharge can substantially change due to precipitation events. In addition, river discharge seasonally varies in many estuaries (Díez-Minguito et al., 2013; Simpson et al., 2001), and spring-neap variations in tidal forcing have a large impact on the extent of the salt intrusion (Banas et al., 2004; Gong et al., 2013; Lerczak et al., 2006).

Such temporal variability in the salt intrusion length indicates that the time-averaged values often do not provide a complete description of the state of estuaries. To address this matter, earlier studies were devoted to quantifying the response of estuaries to time-dependent forcing (Chen, 2015; Kranenburg, 1986; MacCready, 1999, 2007; Monismith et al., 2002). Of particular interest is the statistical behavior of the salt intrusion length in estuaries, for example, described by time-dependent probability density functions (PDFs). To obtain such PDFs, auto-regressive models, in combination with Markov Chain Monte Carlo simulations, were used in the Suwannee River (USA) estuary (Guerra-Chanis et al., 2019) and the Guadalquivir (Spain) estuary (Reyes-Merlo et al., 2013). More detailed statistical models were also introduced to fill the gaps between scarce observational data (Tian, 2019).

In principle, all variability in the salt intrusion length can be traced back to internal processes in the estuary, such as waves or instabilities of density currents, and variability in the forcing, for example, in the river discharge (Biemond et al., 2022; Chen, 2015). Additional understanding of salt intrusion in estuaries would be obtained if we would be able to explain the statistical properties of the salt intrusion length from the statistical properties of the forcing. Here, we only focus on river discharge forcing since it was observed that sub-tidal timescale variability in salt intrusion length is primarily induced by varying river discharge. For instance, Lee and Lwiza (2008) reported that the sub-annual variation of bottom salinity in Chesapeake Bay (USA) is mostly due to changing river discharge. Similar conclusions were presented for the Modaomen (China) estuary (Lin et al., 2019).

When considering variability in salt intrusion length, much of the forcing variability is on smaller time scales than subtidal. Hence, it can be represented as a stochastic process in the widely used deterministic salt-intrusion models (Chen, 2015). This results in models consisting of stochastic differential equations, which are subsequently solved using stochastic calculus (Hanson, 2007; Kloeden & Platen, 1992; Oksendal, 1995). The advantage of these stochastic models is that a whole toolbox is available to study the temporal evolution of the salt intrusion characteristics and the corresponding PDFs.

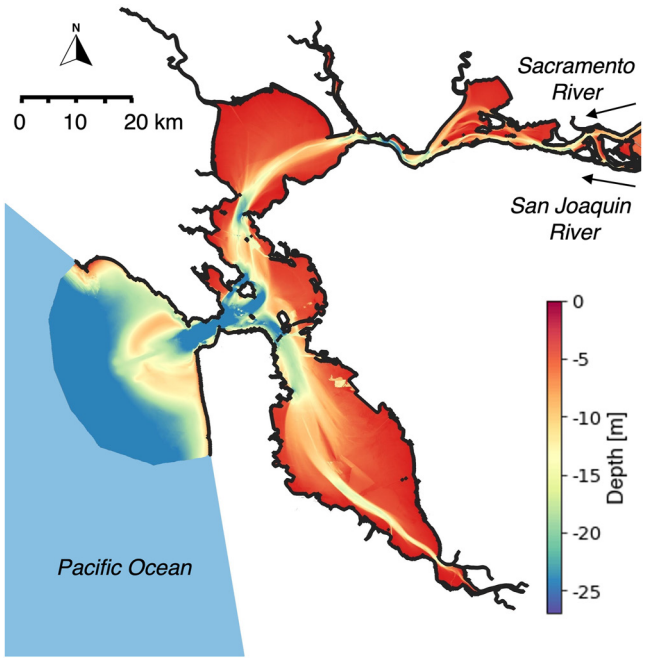

Figure 1. A map of San Francisco Bay, where the bathymetric data is obtained from Fregoso et al. (2017).

In this paper, we formulate conceptual stochastic models of salt intrusion in estuaries and provide, given a stochastic model of the river discharge forcing, solutions for the PDF of the salt intrusion length. First, in Section 2.1 motivating results on the statistics of salt intrusion length and river discharge are presented from observations in the San Francisco Bay (USA) estuary. The general form of a stochastic salt-intrusion model is presented in the remainder of Section 2. Our intention here is to introduce a new view on estuarine salt intrusion, by considering the stochastic forcing-response relationships using the most basic formulation of the physics of estuarine salt intrusion. The San Francisco Bay example serves as a case study and we do not aim to offer a tool which can be used for practical purposes because both the model and observational data set used have substantial limitations.

In Section 3, we consider the stochastic salt intrusion dynamics in this model under different representations of the noise in the river discharge forcing. In the additive noise case, the noise does not depend on the river discharge state itself, whereas in the multiplicative noise case, it does depend on the river discharge state. In Section 4, we show that a more general stochastic model including both additive and multiplicative noise in river discharge, when properly fitted, provides an adequate representation of the skewness of the PDF of the San Francisco Bay salt intrusion length. The results are summarized and discussed in Section 5.

2. Data and Model

Multi-yearly time series of salt intrusion length and river discharge are required to derive reliable sub-tidal statistical properties from observations. Daily river discharge data is available across the globe and can, for example, be downloaded from the Global Runoff Data Centre (GRDC), see https://portal.grdc.bafg.de. There are also large modeling efforts on river discharge and an overview of these models is given in Gao et al. (2020). However, multi-yearly data sets for salt intrusion length are rare. When being evaluated with a sufficient amount of data, salt intrusion lengths can be computed with autoregressive models (Guerra-Chanis et al., 2019; Jassby et al., 1995; Monismith et al., 2002; Reyes-Merlo et al., 2013). The advantage of these models is that the salt intrusion length can be reconstructed even from periods where no observations are available.

2.1. A Motivating Example

As an example, we here use a data set consisting of discharge and salt intrusion length time series from the Dayflow reanalysis product (Ghimire et al., 2022) for San Francisco Bay which was downloaded from https://data.cnra.ca.gov/dataset/dayflow. The complex topography of the San Francisco Bay is shown in Figure 1. Important features for the salt intrusion are the differences in depth between the narrow, deep channel and the shallow parts of the bay in the downstream part, and the confluence of the Sacramento and San Joaquin rivers at about 80 km from the Bay's connection with the ocean. There are many factors that influence the salt intrusion into this estuary (Monismith, 2016; Monismith et al., 2002).

The time series and estimates of the PDF of both river discharge Q and salt intrusion length X_2 (i.e., the distance of the 2 psu isohaline contour to the estuary mouth, see Figure 1) for the San Francisco Bay (Monismith et al., 2002) are plotted versus time t in Figure 2. Based on Monismith et al. (2002), the standard error of the estimates of the salt intrusion length X_2 is 1.32 km (below Equation 8 in his paper). There is a strong seasonal component in both time series with largest river discharge in winter and smallest in summer (Figure 2a), which we will analyze in more detail in Section 4. There are large negative excursions in X_2 when Q has large values (Figure 2b). This leads to a negative skewness in X_2 (Figure 2d) while the PDF of Q is positively skewed (Figure 2c). The dimensionless skewness S calculated here (see values in caption of Figure 2) is the third moment of the time series M_3, normalized by the variance M_2, according to $S = M_3/(M_2)^{3/2}$.

It is important to stress here that the Dayflow time series is not real observational data. In a comparison of the Dayflow salinity data with real observations (e.g., continuously operating bottom salinity sensors), the Dayflow

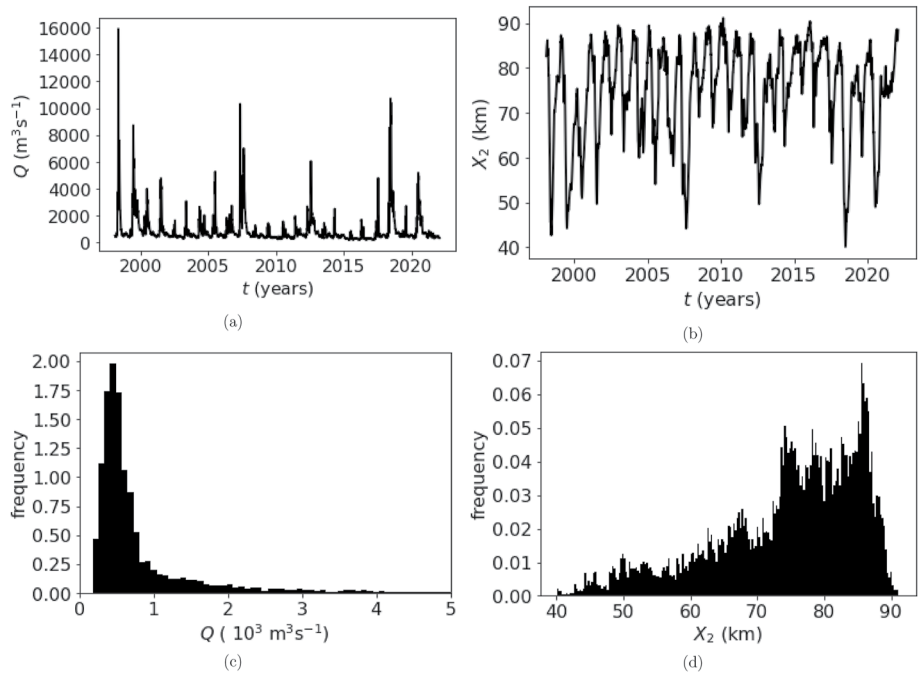

Figure 2. (a) Time series of the river discharge Q for San Francisco Bay over the period 1997–2022. (b) Same but the salt-intrusion length X_2. (c) Histogram of the time series in (a) with mean 893.1 m^3s^{-1}, standard deviation 1,101.1 m^3s^{-1} and skewness 4.6. (d) Same as (c) but for (b) with mean 74.6 km, standard deviation 10.9 km and skewness −0.9. Data source: https://data.cnra.ca.gov/dataset/dayflow.

values deviate systematically from the observed values (Monismith, 2017). This is mainly because the Dayflow estimations are only based on surface observations, and no observations seaward of 55 km are used. A second issue is that, effectively, in the Dayflow salinity data all variability at periods less than 18 days is damped (Monismith, 2017). Also the Dayflow discharge data has limitations for low discharge at sub-monthly time scales, as substantial approximations regarding the water balance have to be made to calculate the net discharge (Monismith, 2016). Finally, during low to moderate flows, regulations and operational constraints play a role. In the last section, we will discuss the effects of these limitations in the Dayflow data on the results for the San Francisco Bay case.

2.2. Stochastic Salt Intrusion Model

One of the simplest deterministic models to determine the sub-tidal salt intrusion characteristic length X in an estuary, given a river discharge Q is that presented in Chen (2015). The governing equation is

$$\frac{1}{2}\frac{dX}{dt} = \frac{C_3}{X^3} + \frac{Q}{A}\left(-1 + \frac{C_2}{X^2}\right) + \frac{C_0}{X} + \left(\frac{Q}{A}\right)^2 \frac{C_1}{X}, \tag{1}$$

where A is the constant cross section of the estuary. The $C_j, j = 0, 1, 2, 3$ are constants that are independent of the river discharge Q. Compared to Chen (2015), partial slip conditions are used on the bottom boundary (instead of no-slip conditions), which leads to the coefficients (Biemond et al., 2022).

$$C_0 = K_h \quad \left[\mathrm{m^2 s^{-1}}\right], \tag{2a}$$

$$C_1 = 0.00305 \times \frac{H^2}{K_v} \quad [\mathrm{s}], \tag{2b}$$

$$C_2 = (0.0275)^2 \times \frac{c^2 H^4}{A_v K_v} \quad \left[\mathrm{m^2}\right], \tag{2c}$$

$$C_3 = (0.0365)^3 \times \frac{c^4 H^6}{A_v^2 K_v} \quad [\mathrm{m^4 s^{-1}}]. \tag{2d}$$

Here, K_h ($\mathrm{m^2 s^{-1}}$) is the horizontal eddy diffusivity, A_v ($\mathrm{m^2 s^{-1}}$) is the vertical eddy viscosity, K_v ($\mathrm{m^2 s^{-1}}$) is the vertical eddy diffusivity, and H (m) is the depth of estuary. Furthermore, $\beta = 7.6 \times 10^{-4}$ (-) is the compressibility of salt, $s_{\mathrm{ocn}} = 35$ (psu) is the prescribed salinity at the river mouth, $g = 9.81$ ($\mathrm{ms^{-2}}$) is the gravitational acceleration and $c = (g\beta s_{ocn} H)^{\frac{1}{2}}$ ($\mathrm{m\ s^{-1}}$). The parameter C_0 controls the strength of the horizontal diffusion of salt. Furthermore, C_1 and C_2 are generally small and quantify the salt intrusion due to the interaction of the shear of the river current with the stratification. Finally, C_3 determines the strength of the salt intrusion due to advection through exchange flow. As it is assumed (Chen, 2015) that the mean salinity varies linearly with the distance to the mouth, we can relate X to X_2 (as plotted in Figure 2b) through $X_2 = (1 - 2/s_{\mathrm{ocn}})X \sim 0.94X$. Note that the sub-tidal model does not account for variations of the salt intrusion length due to the tides, which are estimated in San Francesco Bay to be at most 10 km (Monismith et al., 2002).

In a stochastic salt intrusion model, the river discharge Q_t ($\mathrm{m^3 s^{-1}}$) (the subscript t is added here to explicitly indicate that the variable is stochastic) is determined by the precipitation surplus and snow melt. The magnitudes of these processes have a strong seasonal component, but incidental fluctuations can be large, for example, because of instant heavy rainfall. A conceptual stochastic model for river discharge was suggested in Hoogendoorn and Weltje (2007), with governing equation

$$dQ_t = \lambda_0 Q_t dt + \sigma_0 Q_t dW_t, \tag{3}$$

where W_t is a Wiener process. For further details on stochastic processes such as the Wiener process, we refer to Mikosch (2000). The parameter λ_0 ($\mathrm{s^{-1}}$) is a rate constant and σ_0 ($\mathrm{s^{-1/2}}$) is the discharge volatility. A procedure to estimate the values of these parameters from observations is given in Hoogendoorn and Weltje (2007). A more extended stochastic model of river discharge was presented in Livina et al. (2003), where long-term correlated multiplicative noise replaces the second term in Equation 3 and a periodic forcing is added.

To provide stochastic descriptions of both river discharge and salt intrusion, we generalize Equation 3 and add a stochastic component to Equation 1. This gives stochastic differential equations for the two-dimensional stochastic process (X_t, Q_t).

$$dX_t = 2\left(\frac{C_3}{X_t^3} + \frac{Q_t}{A}\left(-1 + \frac{C_2}{X_t^2}\right) + \frac{C_0}{X_t} + \left(\frac{Q_t}{A}\right)^2 \frac{C_1}{X_t}\right)dt + \sigma_X(t, X_t)dW_t^{(1)}, \tag{4a}$$

$$dQ_t = \mu_Q(t, Q_t)dt + \sigma_Q(t, Q_t)dW_t^{(2)}. \tag{4b}$$

Here the functions μ_Q and σ_Q are kept general for the moment and $\mu_Q(t, Q_t)$ can, for example, include a seasonal component. In Equation 4a, also a general noise term (independent of the river discharge noise) σ_X ($\mathrm{ms^{-1/2}}$) is added for completeness. Such a contribution can result from precipitation and evaporation over the estuary (Savenije, 2005). Although it is considered to be very small, we keep it here as it is useful to illustrate the effects of river discharge noise on the salt intrusion statistics (Section 3.1 below). Hence, in this general formulation, there are two Wiener processes $W_t^{(i)}$, $i = 1, 2$. The initial conditions are $X_0 = X(t_0)$ and $Q_0 = Q(t_0)$.

As written in Equation 4b, the model is formulated as a system of Itô stochastic differential equations, which is most appropriate for numerical calculations (Mikosch, 2000). A Stratonovich formulation could equally well be used and next transformed into Itô equations, but this is not further considered here as it does not influence the results essentially. The Equation 4 are solved with an Euler-Maruyama scheme (Kloeden et al., 1994) over an interval of 20 years, with a time step $\Delta t = 0.11$ days, which gives sufficient accuracy in the numerical solutions (verified by using time steps down to $\Delta t = 0.014$ days). The Python codes of the stochastic salt intrusion model (SSM version) are available online (Dijkstra et al., 2023).

3. Results: Idealized Cases

In this section, we investigate how the statistics of the salt intrusion length responds to different stochastic formulations of the river discharge. To focus on the role of noise on the basic processes of salt intrusion,

two classical limiting cases of Equation 4b will be studied: the diffusive limit (also called the "tidal stirring limit" (MacCready, 2007)), for which $C_1 = C_2 = C_3 = 0$, and the exchange limit, for which $C_0 = C_1 = C_2 = 0$ (Chatwin, 1976).

Values for the depth, width, horizontal diffusion coefficient (for the diffusive limit) and the vertical diffusion coefficient (for the exchange limit) are chosen based on the San Francisco Bay example (Section 2.1). Regarding the geometry, representative values are $H = 13$ m and width $B = 2{,}100$ m. Appropriate values for the mixing coefficients are chosen such that the mean salt intrusion length computed by the model matches the observed mean salt intrusion length. In the observations (Figure 2), the average salt intrusion length $\bar{X}_2 = 74.6$ km (hence $\bar{X} = 79.4$ km), while the average river discharge $\bar{Q} = 893$ m^{3}s^{-1}. To obtain these values in the two limiting cases, $K_h = 2{,}600$ m^{2}s^{-1} is chosen for the diffusive limit and $K_v = 5.5 \times 10^{-4}$ m^{2}s^{-1} for the exchange limit; we will also assume that $A_v = K_v$. Values of the noise amplitudes are chosen arbitrarily here, but are motivated by estimated values from observations, such as presented in Section 4 below.

3.1. Constant Q_t

In this first subsection, we only consider additive noise in Equation 4a, independent of the river discharge. Although this is a physically less interesting case, as this noise contribution is assumed to be small, it serves here to illustrate the methodology as explicit analytical solutions of the PDFs can be obtained. In this case ($Q_t = \bar{Q}$ and constant σ_X), Equation 4a can be written in the form.

$$dX_t = f(X_t)dt + \sigma_X dW_t, \tag{5a}$$

$$f(X) = \begin{cases} 2\left(\dfrac{C_0}{X} - \dfrac{\bar{Q}}{A}\right) & \text{(diffusive limit)}, \\ 2\left(\dfrac{C_3}{X^3} - \dfrac{\bar{Q}}{A}\right) & \text{(exchange limit)}, \end{cases} \tag{5b}$$

where only the two limiting cases are considered.

The PDF, indicated from now on by $p\,(x, t)$, satisfies the Fokker-Planck equation (Gardiner, 2002)

$$\frac{\partial p}{\partial t} = -\frac{\partial}{\partial x}(f(x)p) + \frac{\sigma_X^2}{2}\frac{\partial^2 p}{\partial x^2}, \tag{6}$$

on the domain $(x, t) \in [0, \infty] \times [0, \infty]$ with $p \to 0$ for $x \to \infty$. The equilibrium solution $p_e(x)$ of Equation 6 is given by

$$p_e(x) = N\exp\left(\int_0^x \frac{2}{\sigma_X^2} f(s)\ ds\right) \tag{7}$$

and N is a normalization constant such that $\int_0^\infty p_e(x)dx = 1$.

For the deterministic exchange limit case ($\sigma_X = 0$), and the value of $K_v = 5.5 \times 10^{-4}$ m^{2}s^{-1} chosen, the model gives a salt intrusion length of $X = 79.1$ km. A typical time series of salt intrusion length for $\sigma_X = 0.03$ (km s$^{-1/2}$) is shown in Figure 3a. The histogram and analytical PDF (Equation 7, red curve) are plotted in Figure 3b. Under constant river discharge X is positively skewed, with large positive excursions of X, due to the nonlinear processes in the salt balance equation. For the deterministic diffusive limit, and the value of $K_h = 2{,}600$ m^{2}s^{-1} chosen, the model gives a salt intrusion length of $X = 79.5$ km. For $\sigma_X = 0.03$ (km s$^{-1/2}$) the results show similar positive skewness (Figures 3c and 3d) as in the exchange flow case, but with a larger variance.

The mechanism explaining the positive skewness is the fact that the damping of the fluctuations in salt intrusion length (with respect to the mean), say indicated by $\tilde{X}$, is expressed as the derivative of the function $f(X)$ in Equation 5b at the mean salt intrusion length $\bar{X}$. This results from linearization of the Equation 5b around $\bar{X}$, resulting in an equation $d\tilde{X} \sim \lambda\tilde{X}dt$, where λ is a damping coefficient. For the diffusive limit, λ is proportional to $-C_0/\bar{X}^2$. If $\bar{X}$ is large, then λ is small and so large excursions of X can occur. If $\bar{X}$ is small, there is large damping, preventing large excursions. For the exchange limit, the damping is proportional to $-C_3/\bar{X}^4$ and hence a similar reasoning explains the positive skewness.

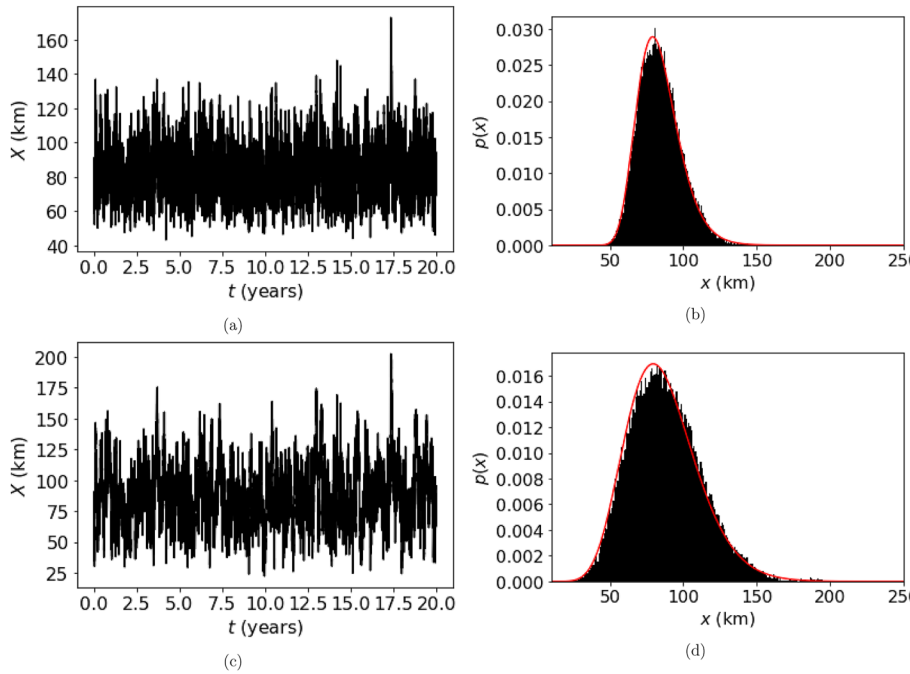

Figure 3. (a) Time series of the salt intrusion length X for the constant Q, San Francisco Bay case for $\sigma_X = 0.03$ (km s$^{-1/2}$) in the exchange limit. (b) Histogram of the time series in (a) with mean 84.4 km, standard deviation 14.7 km and skewness 0.63. The analytic PDF (7) is the red curve. (c)–(d) Same as (a) and (b) but then for the diffusive limit and with $\sigma_X = 0.03$ (km s$^{-1/2}$). In this case, we find a mean 87.8 km, standard deviation 24.5 km and skewness 0.51.

Note that a positively skewed distribution in the salt intrusion length is not seen in the salt intrusion length measurements in Figure 2d. Below, we will investigate whether variability in the river discharge Q might explain the observed negative skewness.

3.2. Stochastic Q_t: Additive Noise

To consider the effects of additive noise in the river discharge Q, with mean $\bar{Q}$, on X we choose μ_Q and σ_Q in Equation 4b as

$$\mu_Q(t, Q_t) = \frac{\bar{Q} - Q_t}{\tau} \tag{8a}$$

$$\sigma_Q(t, Q_t) = \sigma\bar{Q} \tag{8b}$$

where τ (s^{-1}) is a damping time scale and σ (s$^{-1/2}$) a constant normalized standard deviation. With introduction of the new variable $Y_t = \left(Q_t - \bar{Q}\right)/\bar{Q}$, the equations for X_t and Y_t become

$$dX_t = \begin{cases} 2\left(\dfrac{C_0}{X_t} - \dfrac{\bar{Q}(1+Y_t)}{A}\right)dt + \sigma_X dW_t^{(1)} & \text{(diffusive limit)}, \\ 2\left(\dfrac{C_3}{X_t^3} - \dfrac{\bar{Q}(1+Y_t)}{A}\right)dt + \sigma_X dW_t^{(1)} & \text{(exchange limit)}, \end{cases} \tag{9a}$$

$$dY_t = -\frac{Y_t}{\tau}dt + \sigma dW_t^{(2)}. \tag{9b}$$

In this case, Y_t is an Ornstein-Uhlenbeck process (or red noise process) with equilibrium covariance function proportional to exp $(-t/\tau)$ (Mikosch, 2000). The equilibrium PDF of Q_t is Gaussian with mean $\bar{Q}$ and variance $\bar{Q}^2\tau\sigma^2/2$.

We consider the two limiting cases for the San Francisco Bay estuary, with $\tau = 10$ (days) and $\sigma = 10^{-4}$ (s$^{-1/2}$). Indeed, the simulated Q (Figures 4a and 4b) has a near-Gaussian distribution (a longer time series is needed to

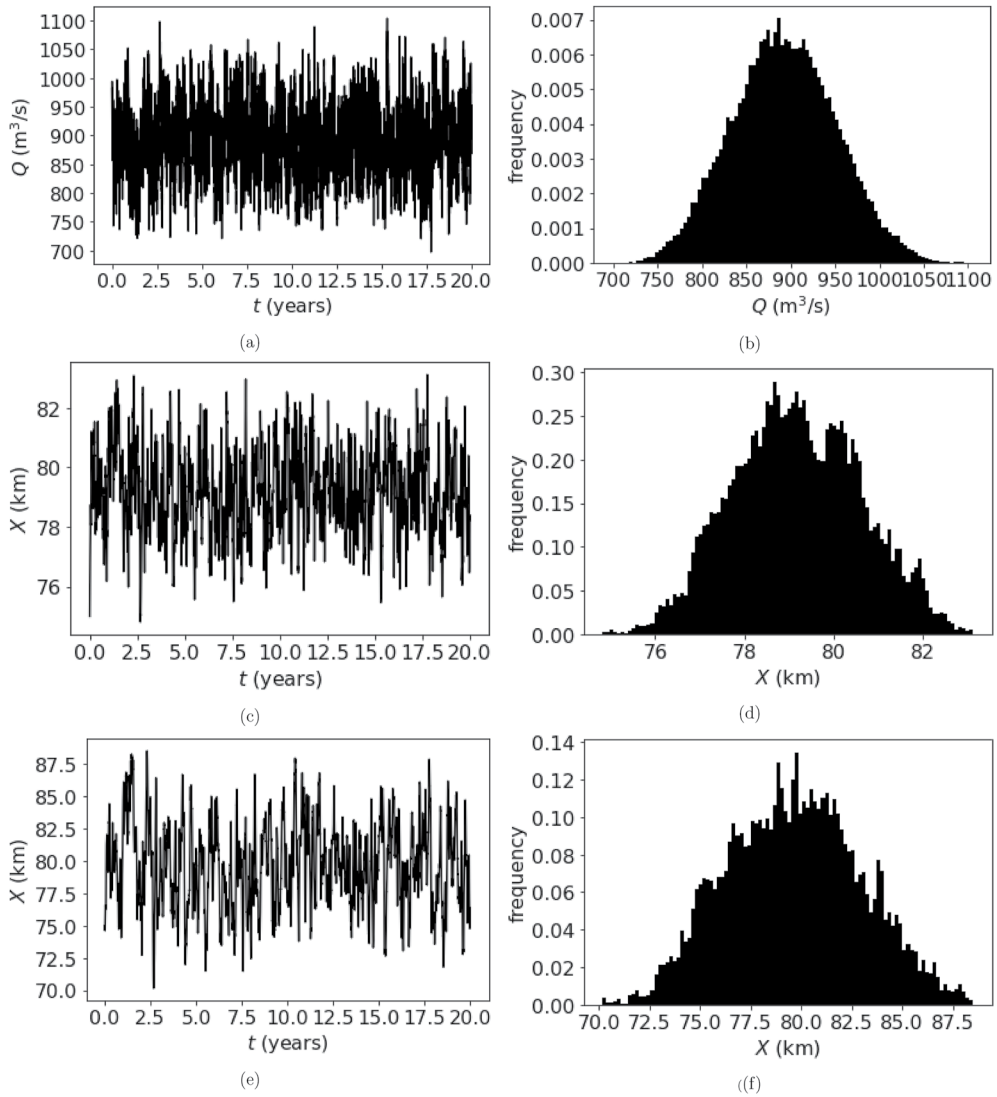

Figure 4. (a) Time series of river discharge Q for red noise with $\tau = 10$ days and $\sigma = 10^{-4}$ ($s^{-1/2}$). (b) Histogram of the time series of (a) with mean 892.6 m^3s^{-1}, standard deviation 58.6 m^3s^{-1} and skewness 5.7×10^{-2}. (c) Time series of the salt intrusion length X in the exchange limit case; note that $\sigma_X = 0$. (d) Histogram of the time series in (c) with mean 79.2 km, standard deviation 1.4 km and skewness 3.6×10^{-2}. (e) Same as (c) but for the diffusive limit case. (f) Histogram of the time series in (e) with mean 79.6 km, standard deviation 3.3 km and skewness 5.1×10^{-2}.

obtain a zero skewness). In the exchange limit (Figures 4c and 4d), there is a slight positive skewness in the results for X due to the same mechanism as in the constant Q case (Section 3.1). The standard deviation of both Q and X increases substantially with increasing τ (results not shown) as is expected from the Ornstein-Uhlenbeck process for Q. The results for the diffusive limit (Figures 4e and 4f) are very similar to the exchange flow case with again a larger variance in the distribution for X.

White noise is obtained in the limit $\tau \to 0$ and Q_t can be written as

$$Q_t = \bar{Q}(1 - \sigma\zeta(t)) \to Y_t = -\sigma\zeta(t), \tag{10}$$

where $\zeta(t)$ is a white noise (Mikosch, 2000) process (zero mean and delta correlated). The equation for X_t then becomes

$$dX_t = f(X_t)dt + \sigma_X dW_t^{(1)} + 2\frac{\bar{Q}}{A}\sigma dW_t^{(2)}, \tag{11a}$$

$$f(X) = \begin{cases} 2\left(\frac{C_0}{X_t} - \frac{\bar{Q}}{A}\right), & \text{(diffusive limit).} \\ 2\left(\frac{C_3}{X_t^3} - \frac{\bar{Q}}{A}\right), & \text{(exchange limit).} \end{cases} \tag{11b}$$

Hence, when only a single realisation of the Wiener process is considered ($W^{(1)} = W^{(2)}$), the white noise case is the same as the constant Q case with $\sigma'_X = \sigma_X + 2\sigma\bar{Q}/A$ and hence the results are similar to those in Section 3.1 (and hence not shown).

3.3. Varying Q_t: Multiplicative Noise

Next, the noise in the river discharge is assumed proportional to Q itself. This is considered to be a reasonable assumption (Hoogendoorn & Weltje, 2007) as in case of large discharge, many sources of discharge are involved and hence fluctuations are also large. For small discharge, there are only a few sources and fluctuations are smaller. To obtain pure multiplicative noise, we choose in Equation 4b.

$$\mu_Q(t, Q_t) = \frac{\bar{Q} - Q_t}{\tau} \tag{12a}$$

$$\sigma_Q(t, Q_t) = \sigma\left(Q_t - \bar{Q}\right) \tag{12b}$$

with constant τ and constant σ. Again with $Y_t = \left(Q_t - \bar{Q}\right)/\bar{Q}$, this gives

$$dY_t = \mu Y_t dt + \sigma Y_t dW_t^{(2)}. \tag{13}$$

with the notation $\mu = -1/\tau$ to make the formulas below easier. The stochastic model for Y_t (which is a geometric Brownian motion process in the Itô case), has a corresponding Fokker-Planck equation

$$\frac{\partial p}{\partial t} = -\frac{\partial}{\partial y}(\mu y p) + \frac{\partial^2}{\partial y^2}\left(\frac{y^2\sigma^2}{2}p\right). \tag{14}$$

The time-dependent solution $p\,(y, t)$, for $y \geq 0$, with initial condition $p\,(y, 0) = p_0(y)$ is given by

$$p(y,t) = \frac{p_0(y)}{y\sqrt{2\pi\sigma^2 t}} e^{-\frac{\left(\ln y - \mu t + \frac{1}{2}\sigma^2 t\right)^2}{2\sigma^2 t}}, \tag{15}$$

and hence the stochastic variable $Z_t = \ln Y_t$ is normally distributed with mean $\mu t - \sigma^2 t/2$ and variance $\sigma^2 t$. The mean (and other moments) of this distribution are thus not stationary, which is not a satisfactory model for river discharge (as also acknowledged in Hoogendoorn & Weltje, 2007).

To obtain stationary statistics, we consider the Correlated Additive-Multiplicative (CAM) noise model where the PDF is of power-law type (Castellana et al., 2018; Sura et al., 2001). Suggestions for power-law distributions of river discharge have also appeared frequently in the literature (Bowers et al., 2012) and see references in Livina et al. (2003). The equation for Y_t in this case becomes

$$dY_t = \mu Y_t dt + (\sigma_A + \sigma_M Y_t) dW_t^{(2)}, \tag{16}$$

with two noise amplitudes σ_A (additive) and σ_M (multiplicative). The additive component could arise from random storage of water in a river due to soil or vegetation variations (Hickin, 1984) in addition to human induced variations (all independent of the river discharge itself). The corresponding Fokker-Planck equation to Equation 16 is

$$\frac{\partial p}{\partial t} = -\frac{\partial}{\partial y}(\mu y p) + \frac{1}{2}\frac{\partial^2}{\partial y^2}\left[(\sigma_A + \sigma_M y)^2 p\right]. \tag{17}$$

The equilibrium PDF for $y > -\sigma_A/\sigma_M$ is given by (Castellana et al., 2018; Sura et al., 2001)

$$p_e(y) = N \exp\left\{\frac{2\mu}{\sigma_M^2}\left[\left(1 - \frac{\sigma_M^2}{\mu}\right)\ln(|\sigma_M y + \sigma_A|) + \frac{\sigma_A}{\sigma_M y + \sigma_A}\right]\right\} \tag{18}$$

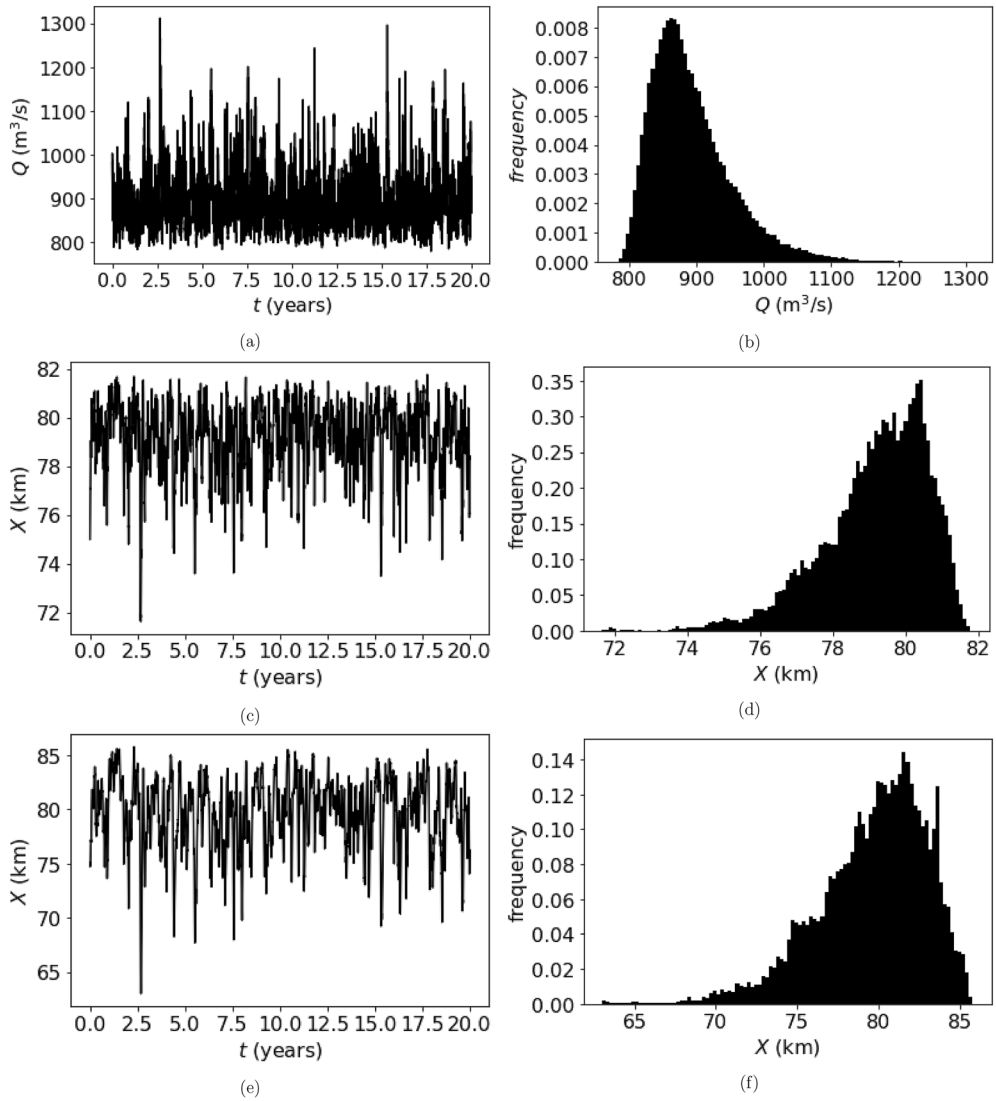

Figure 5. (a) Time series of river discharge Q for Correlated Additive-Multiplicative noise with $\tau = 10$ days and $\sigma_A = 10^{-4}$ ($s^{-1/2}$) and $\sigma_M = 5 \times 10^{-4}$ ($s^{-1/2}$). (b) Histogram of the time series of (a) with mean 892.6 $m^3 s^{-1}$, standard deviation 61.3 $m^3 s^{-1}$ and skewness 1.3. (c) Time series of the salt intrusion length X in the exchange limit case; note that $\sigma_X = 0$. (d) Histogram of the time series in (c) with mean 79.2 km, standard deviation 1.4 km and skewness −1.02. (e) Same as (c) but for the diffusive limit case. (f) Histogram of the time series in (e) with mean 79.7 km, standard deviation 3.4 km and skewness −0.88.

and $p_e(y) = 0$ when $y \leq -\sigma_A/\sigma_M$; here N is again a normalization constant such that the integral over $p_e(y)$ is unity.

By coupling Equation 16 to the stochastic salt intrusion model Equation 9a, we can systematically address the effects of the multiplicative noise. Note that for $\sigma_M = 0$, we recover the additive noise case with a damping time scale τ and noise amplitude $\sigma_A = \sigma$. Results are shown in Figure 5 for $\tau = 10$ days, $\sigma_A = 10^{-4}$ ($s^{-1/2}$) and $\sigma_M = 5 \times 10^{-4}$ ($s^{-1/2}$). As soon as multiplicative noise is present, the negative skewness in the PDF of X is found in the exchange limit (Figures 5c and 5d) under a positive skewness in Q (Figures 5a and 5b). This can be explained by the fact that the noise-driven excursions in Q become proportional to the discharge, leading to large positive excursions in the discharge and consequently negative ones in the salt intrusion length. Similar results are also found in the diffusive limit case (Figures 5e and 5f), but the PDF for salt intrusion length in this case has a larger spread than that in the exchange flow case.

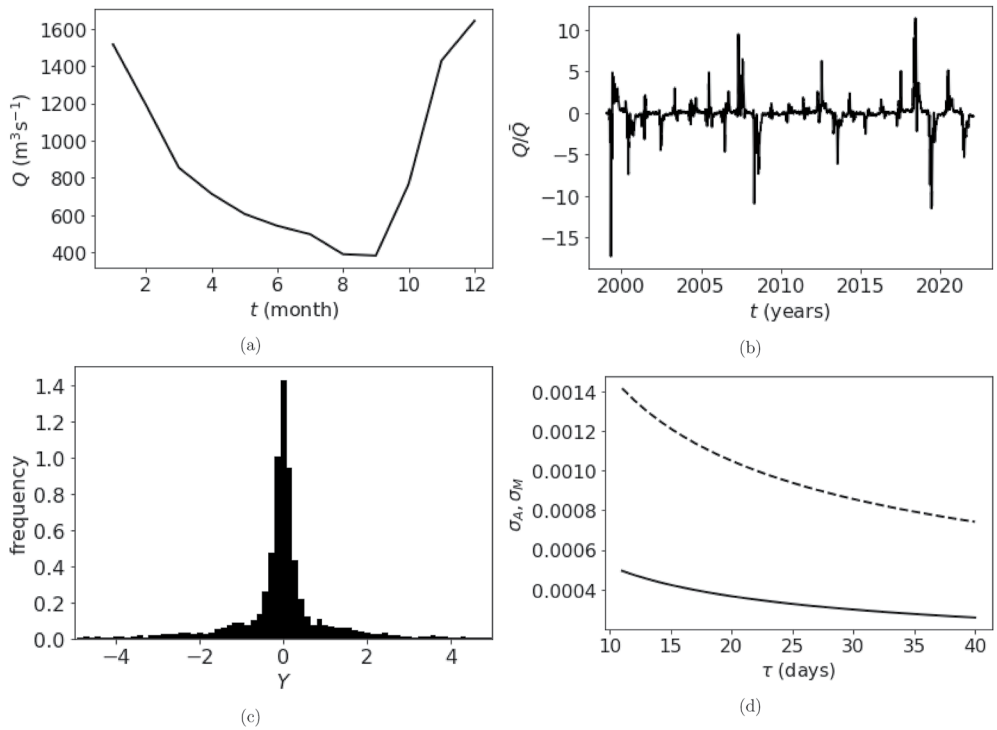

Figure 6. (a) Mean seasonal cycle of the time series in Figure 2a. (b) Time series of the seasonally filtered data. (c) Histogram of the time series in (c). (d) Variation of the noise amplitudes σ_A (drawn) and σ_M (dashed), both in $s^{-1/2}$, in the Correlated Additive-Multiplicative model versus the decay time scale τ in the autocorrelation function.

4. Results: San Francisco Bay Case

So far, we have only considered the idealized exchange and diffusive limits and focussed on typical qualitative results, not worrying about the precise amplitudes of the noise and neglecting any seasonal dependence of the river discharge. To investigate whether the stochastic model defined by Equation 4 is able to capture the statistics of the San Francisco Bay salt intrusion lengths, as shown in Section 2.1, we turn to the model with CAM noise as in Section 3.3 and add a seasonal component in the river discharge forcing. The equations then become

$$dX_t = 2\left(\frac{C_3}{X_t^3} + \frac{Q_t}{A}\left(-1 + \frac{C_2}{X_t^2}\right) + \frac{C_0}{X_t} + \left(\frac{Q_t}{A}\right)^2 \frac{C_1}{X_t}\right)dt + \sigma_X dW_t^{(1)}, \tag{19a}$$

$$dY_t = (\mu Y_t + S_Y(t))dt + (\sigma_A + \sigma_M Y_t)dW_t^{(2)}, \tag{19b}$$

where the seasonal component is represented by $S_Y(t)$. Parameterizations for the viscosities and diffusivities used are (Biemond et al., 2022)

$$K_v = 7.28\ \ 10^{-5} \times U_T H\ \ ;\ \ A_v = \frac{K_M}{Sc}\ \ ;\ \ K_h = 0.035 \times U_T H, \tag{20}$$

where $U_T = 0.85$ (ms^{-1}) is the tidal current amplitude and $Sc = 2.2$ is the Schmidt number.

To estimate parameters in the stochastic river discharge model Equation 19b, we first analyze the seasonal mean in the observed time series and the probability density of the seasonally filtered data, the latter calculated by differencing the original time series. The seasonal cycle of the river discharge Q shows maximal values in December-January and minimal values around August-September (Figure 6a). We fit this seasonal cycle rather roughly with a simple function $S_Q(t) - \bar{Q} = a\sin(2\pi t/T) + b\cos(2\pi t/T)$, with coefficients $a = 203$ m^{3}s^{-1}, $b = 520$ m^{3}s^{-1} and T is 1 year. This results in the function $S_Y(t) = \alpha\cos(2\pi t/T) + \beta\sin(2\pi t/T)$, where $\alpha = -2a\pi/(T\bar{Q}) = -4.38 \times 10^{-8}$ (s^{-1}) and $\beta = 2\pi b/(T\bar{Q}) = 1.12 \times 10^{-7}$ (s^{-1}).

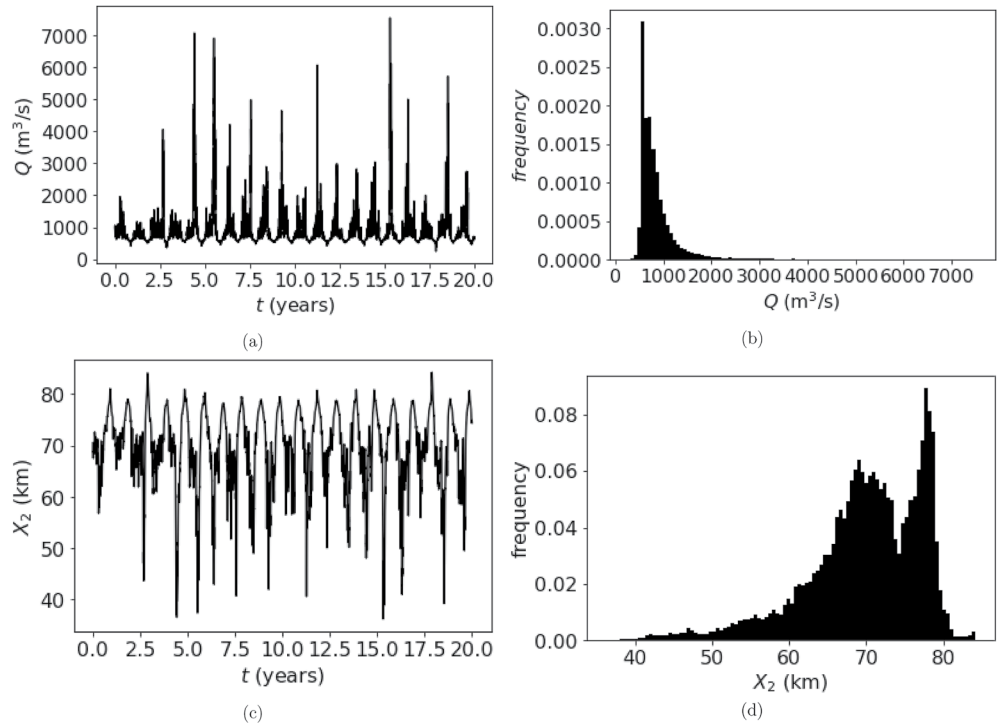

Figure 7. (a) Full model with Correlated Additive-Multiplicative noise for the San Francisco Bay estuary, with $\tau = 20$ days, $\sigma_X = 0$, $\sigma_A = 3.66 \times 10^{-4}$ ($s^{-1/2}$) and $\sigma_M = 1.05 \times 10^{-3}$ ($s^{-1/2}$). (a) Time series of Q. (b) Histogram of the time series in (a) with mean 887.4 m^3s^{-1}, standard deviation 517.7 m^3s^{-1} and skewness 4.1. (c) Time series of X_2. (d) Histogram for the time series in (c) with mean 74.3 km, standard deviation 8.1 km and skewness −1.1.

The seasonally filtered time series are shown in Figure 6b and its histogram (Figure 6c) shows a non-Gaussian shape. The decay time scale τ is determined from the computation of the autocorrelation function of the time series in Figure 6b and gives about 20 days. This appears to be reasonable value considering the adjustment time scales of river discharge to large rainfall anomalies (Savenije, 2005). Having determined τ, this fixes $\mu = -1/\tau$. We next fit a CAM noise model to this time series, by assuming that the seasonally filtered data are stationary and hence the moments M_j, $j = 1, \ldots 3$ of this distribution can be fitted to those of Equation 18 which are given by (Castellana et al., 2018)

$$M_1 = 0 \;;\; M_2 = -\frac{\sigma_A^2}{2\mu + \sigma_M^2} \;;\; M_3 = \frac{2\sigma_A^3 \sigma_M}{\left(2\mu + \sigma_M^2\right)\left(\mu + \sigma_M^2\right)}. \tag{21}$$

The variation of the coefficients σ_A and σ_B with the chosen decay time scale τ is shown in Figure 6d. Because the amplitude σ_M is larger than σ_A, this indicates that multiplicative noise is important to explain the river discharge statistics (of course, under the assumptions of a CAM noise stochastic model).

One can now systematically study the behavior of the salt intrusion model by first considering the case $\mu = \sigma_M = \sigma_A = \sigma_X = 0$ to check whether the seasonal cycle is well simulated. As another case, the seasonal cycle can be switched off ($\alpha = \beta = 0$) to check whether the distribution in Y as in Figure 6c is generated, with the estimated values of μ, σ_A, and σ_M. Although we do not show results of these simulations here, the results are instructive to determine how noise and seasonal forcing contribute to variability in salt intrusion.

With full seasonal cycle, $\tau = 20$ days, $\sigma_X = 0$ and the fitted values of $\sigma_A = 3.66 \times 10^{-4}$ ($s^{-1/2}$) and $\sigma_M = 1.05 \times 10^{-3}$ ($s^{-1/2}$), the results for the river discharge and salt-intrusion length $X_2 = 0.94X$ are shown in Figure 7. The river discharge distribution (cf. Figure 2c) is relatively well represented, although the large extremes in discharge (cf. Figure 2a) are not captured. Also the salt intrusion length PDF (cf. Figure 2d) is reasonably captured, in particular the negative skewness. No effort was undertaken to further optimize the parameters to get an even closer correspondence with the observed salt intrusion length PDF, as also the salt intrusion model is quite idealized.

Changes in the damping time scale τ affect the PDF quantitatively but in the range of realistic values ($\tau = 10 - 30$ days), the negative skewness in X_2 is still captured well. This shows that the stochastic model in Section 2.2, with CAM noise in the river discharge, is capable to efficiently represent the statistics of both river discharge and salt intrusion length. A nonzero σ_X will add to the variability of the salt intrusion length, but as its magnitude is likely to be very small (Savenije, 2005), we do not consider this effect here.

5. Summary and Discussion

In many salt intrusion modeling studies in estuarine environments, deterministic models are used and the position of the salt intrusion front is estimated given forcing conditions, such as river discharge (Martyr-Koller et al., 2017). Focus is often on the different flow regimes which can appear in parameter space (Dijkstra & Schuttelaars, 2021; Geyer & MacCready, 2014) or on the transient response to river discharge variability (Biemond et al., 2022; Monismith et al., 2002). Indeed, to determine the statistics of the salt intrusion length, one can force any salt-intrusion model with an observed time series of river discharge (or a statistical model of such a time series) and investigate the salt response. In this paper, we introduced an idealized stochastic model of the combined river discharge behavior and salt intrusion length in estuaries. Instead of just prescribing the river discharge, stochastic models of river discharge were proposed, following up on the work of Hoogendoorn and Weltje (2007) and Livina et al. (2003). By doing so, the effects of the stochastic properties in the river discharge time series on the statistics (e.g., Gaussian vs. non-Gaussian) of the salt intrusion length can be systematically studied.

Key to formulate such stochastic models is the representation of the noise in the forcing and/or the stochastic representation of non-resolved processes, such as mixing. In this study, we restricted the analysis to stochastic representation of the river discharge forcing for which we used well-known stochastic models (e.g., red noise) with its special limiting cases (e.g., white noise). This representation was combined with a stochastic conceptual nonlinear salt-intrusion model. Only diffusion processes were used in the stochastic models to which standard Itô calculus can be applied. The use of additive and multiplicative noise processes in the river discharge model was interpreted through the representation of specific processes, where the additive component is viewed as the representation of the random variations in water storage, for example, due to vegetation changes (Hickin, 1984), and the multiplicative component through the variations of discharge due to multiple sources (Hoogendoorn & Weltje, 2007). In the salt-intrusion results, we focussed on qualitative properties of the probability density function (PDF) of the salt intrusion length, in particular on its non-Gaussian properties (e.g., skewness). In specific cases, analytical representations of the PDF could be obtained by solving the corresponding Fokker-Planck equation.

Two dynamically limiting cases, the exchange limit and the diffusive limit, were considered in the salt balance equation. When, for each limiting case, fluctuations in the river discharge are modeled as red noise (i.e., with a Gaussian PDF) this leads to a positive skewness in the salt intrusion length PDF. The reason is that the salt-intrusion responds differently to small river discharges than to large ones. The degree of the skewness depends on the decorrelation time scale of the river discharge. For Correlated Additive-Multiplicative (CAM) noise (Sura et al., 2001) in the river discharge, the skewness becomes strongly negative because noise in the river discharge is strongly amplified at large discharges and leads to large negative excursions in the salt intrusion length. The CAM noise model is generalizing earlier work on stochastic river discharge modeling (Hoogendoorn & Weltje, 2007), although the actual time series of many rivers may show more complicated behavior (Livina et al., 2003).

With a seasonal forcing and CAM noise parameters based on observations, the statistics of salt intrusion in the San Francisco Bay estuary could be reasonably captured and understood. We reiterate that the Dayflow data has several limitations (Section 2.1) in particular on sub-monthly values of river discharge and salt intrusion length (Monismith, 2016). As we focus in this paper on the multi-year statistical properties, these data limitations will not have much effect on these results as variability on sub-monthly time scales has a much smaller amplitude than that on the longer time scales. The salt intrusion model also has limitations in describing the salt intrusion in the San Francisco Bay estuary. To provide a more detailed description of the statistics of the salt intrusion of this particular example other, for example, more empirical models (Monismith, 2017), can be used.

The approach can be extended to compute the two-dimensional PDF in the river discharge, salt intrusion length space, by solving a spatially two-dimensional Fokker-Planck equation, and can then be compared to results on

functional relationships between these variables, such as provided in Figure 4 of Monismith et al. (2002). The methodology was also applied to the Quadalquivir giving qualitatively similar results for the PDFs as for the San Francisco Bay case. The observed PDFs of the Quadalquivir, however, have a bimodal shape due to the water management of the estuary and hence are not fully captured by our model. Hence, if one is interested in reproducing the detailed statistical properties of salt intrusion in a specific estuary, one may have to turn to more complicated stochastic models for river discharge, for example, with help of nonlinear time series analysis methods (Livina et al., 2003). In principle the methodology presented in this paper can also be applied to establish a statistical relationship between forcing conditions (e.g., discharge) and salinity in a branched system. However, this would require considering other quantities as done now, since the extent of salt intrusion and discharge in a branched system differs per branch. Moreover, the model would need modifications to be suitable to simulate branched systems. Physics that need to be included would be quite different when the salt intrusion extends beyond a bifurcation.

Further work could focus on the application to more detailed salt intrusion models The stochastic approach can certainly be extended to 2DV models, which are formulated by stochastic partial differential equations. Techniques exist to efficiently solve such equations numerically. For instance, to decrease the dimensionality of the system, a Karhunen-Loeve expansion can be performed on the stochastic variables (Holmes et al., 2012; Sapsis & Lermusiaux, 2009). Also the class of stochastic processes can be extended, for example, with the inclusion of jump processes (Hanson, 2007) in addition to diffusion processes, to generate possibly better representations for river discharge which are related to extreme rainfall events or extreme droughts. Note that once such a stochastic model has been developed, one can use it to study the long-term changes in salt intrusion length statistics, for example, due to climate change, by determining how the parameters in the stochastic model of the river discharge will change. In this way, also changes in extremes in salt intrusion length under climate change can be efficiently determined.

Although the intend of the paper was to introduce the stochastic methodology in the estuary physics community, we think that it can also be of practical use. One problem that could be addressed is how to change the statistics of the river discharge Q (which could in reality be achieved through upstream water regulation) to obtain statistics of X_2 that obey user-specified criteria. For example, an explicit criterion could be that at a specific spatial distance X_* from the estuary mouth, the probability that $X_2 > X_*$ is below a given critical value. Likewise, one could use this to demand that the mean time interval of events during which $X_2 > X_*$ is below a critical value. In this way, the methodology may eventually be useful for water management purposes.

Data Availability Statement

The measured river discharge and salt intrusion length, used in the analysis of this paper, are retrieved from https://data.cnra.ca.gov/dataset/dayflow for the San Francisco Bay. All codes to generate the results can be downloaded (Dijkstra et al., 2023) from https://zenodo.org/record/8006697#.ZH8M8C8RrEk, DOI: https://doi.org/10.5281/zenodo.8006697.

Acknowledgments
This work is part of the Perspectief Program SaltiSolutions, which is financed by the Dutch Research Council (NWO) Domain Applied and Engineering Sciences (2022/TTW/01344701) in collaboration with private and public partners.

References

Banas, N. S., Hickey, B. M., MacCready, P., & Newton, J. A. (2004). Dynamics of willapa bay, Washington: A highly unsteady, partially mixed estuary. *Journal of Physical Oceanography*, *34*(11), 2413–2427. https://doi.org/10.1175/JPO2637.1

Biemond, B., De Swart, H. E., Dijkstra, H. A., & Díez-Minguito, M. (2022). Estuarine salinity response to freshwater pulses. *Journal of Geophysical Research: Oceans*, *127*, e2022JC018669. https://doi.org/10.1029/2022JC018669

Bowers, M. C., Tung, W. W., & Gao, J. B. (2012). On the distributions of seasonal river flows: Lognormal or power law? *Water Resources Research*, *48*(5), W05536. https://doi.org/10.1029/2011WR011308

Castellana, D., Dijkstra, H. A., & Wubs, F. W. (2018). A statistical significance test for sea-level variability. *Dynamics and Statistics of the Climate System*, *3*, dzy008. https://doi.org/10.1093/climsys/dzy008

Chatwin, P. (1976). Some remarks on the maintenance of the salinity distribution in estuaries. *Estuarine and Coastal Marine Science*, *4*(5), 555–566. https://doi.org/10.1016/0302-3524(76)90030-X

Chen, S.-N. (2015). Asymmetric estuarine responses to changes in river forcing: A consequence of nonlinear salt flux. *Journal of Physical Oceanography*, *45*(11), 2836–2847. https://doi.org/10.1175/JPO-D-15-0085.1

Díez-Minguito, M., Contreras, E., Polo, M., & Losada, M. (2013). Spatio-temporal distribution, along-channel transport, and post-riverflood recovery of salinity in the Guadalquivir estuary (SW Spain). *Journal of Geophysical Research: Oceans*, *118*(5), 2267–2278. https://doi.org/10.1002/JGRC.20172

Dijkstra, H. A., Biemond, B., Lee, J., & De Swart, H. E. (2023). Stochastic salt intrusion model (SSM), v1.0 [Software]. https://doi.org/10.5281/zenodo.8006697

Dijkstra, Y. M., & Schuttelaars, H. M. (2021). A unifying approach to subtidal salt intrusion modeling in tidal estuaries. *Journal of Physical Oceanography*, *51*(1), 147–167. https://doi.org/10.1175/JPO-D-20-0006.1

Eslami, S., Hoekstra, P., Minderhoud, P. S., Trung, N. N., Hoch, J. M., Sutanudjaja, E. H., et al. (2021). Projections of salt intrusion in a mega-delta under climatic and anthropogenic stressors. *Communications Earth & Environment*, *2*(1), 1–11. https://doi.org/10.1038/s43247-021-00208-52

Fregoso, T., Wang, R.-F., Alteljevich, E., & Jaffe, B. (2017). San Francisco bay-delta bathymetric/topographic digital elevation model. (technical Report). U.S. Geological Survey. https://doi.org/10.5066/F7GH9G27

Gao, C., Su, B., Krysanova, V., Zha, Q., Chen, C., Luo, G., et al. (2020). A 439-year simulated daily discharge dataset (1861–2299) for the upper Yangtze River, China. *Earth System Science Data*, *12*(1), 387–402. https://doi.org/10.5194/essd-12-387-2020

Gardiner, C. W. (2002). *Handbook of stochastic methods* (2nd ed.). Springer.

Geyer, W. R., & MacCready, P. (2014). The estuarine circulation. *Annual Review of Fluid Mechanics*, *46*, 175–197. https://doi.org/10.1146/annurev-fluid-010313-141302

Ghimire, G. R., Hansen, C. H., Gangrade, S., Kao, S.-C., Thornton, P. E., & Singh, S. (2022). Dayflow: CONUS daily streamflow reanalysis. Version 1. HydroSource. https://doi.org/10.21951/Dayflow/1847639

Gong, W., Shen, J., & Jia, L. (2013). Salt intrusion during the dry season in the Huangmaohai estuary, Pearl river delta, China. *Journal of Marine Systems*, *111–112*, 235–252. https://doi.org/10.1016/j.jmarsys.2012.11.006

Guerra-Chanis, G. E., Reyes-Merlo, M. A., Díez-Minguito, M., & Valle-Levinson, A. (2019). Saltwater intrusion in a subtropical estuary. *Estuarine, Coastal and Shelf Science*, *217*, 28–36. https://doi.org/10.1016/j.ecss.2018.10.016

Hanson, F. B. (2007). *Applied stochastic processes and control for jump-diffusions*. SIAM.

Hickin, E. J. (1984). Vegetation and river channel dynamics. *Canadian Geographer*, *28*(2), 111–126. https://doi.org/10.1111/j.1541-0064.1984.tb00779.x

Holmes, P., Lumley, J. L., Berkooz, G., & Rowley, C. W. (2012). *Turbulence, coherent structures, dynamical systems and symmetry*. Cambridge University Press.

Hoogendoorn, R. M., & Weltje, G. J. (2007). A stochastic model for simulating long time series of river-mouth discharge and sediment load. In S. Begum, M. Stive, & J. W. Hall (Eds.), *Flood risk management in europe, innovation in policy and practice* (pp. 311–331). Springer-Verlag.

Jassby, A. D., Kimmerer, W. J., Monismith, S. G., Armor, C., Cloern, J. E., Powell, T. M., et al. (1995). Isohaline position as a habitat indicator for estuarine populations. *Ecological Applications*, *5*(1), 272–289. https://doi.org/10.2307/1942069

Kloeden, P., & Platen, E. (1992). *Numerical solution of stochastic differential equations*. Springer. https://doi.org/10.1007/978-3-662-12616-5

Kloeden, P., Platen, E., & Schurz, H. (1994). *Numerical solution of stochastic differential equations through computer experiments*. Springer-Verlag.

Kranenburg, C. (1986). A time scale for long-term salt intrusion in well-mixed estuaries. *Journal of Physical Oceanography*, *16*(7), 1329–1331. https://doi.org/10.1175/1520-0485(1986)016<1329:atsflt>2.0.co;2

Lee, Y. J., & Lwiza, K. M. (2008). Factors driving bottom salinity variability in the Chesapeake Bay. *Continental Shelf Research*, *28*(10), 1352–1362. https://doi.org/10.1016/j.csr.2008.03.016

Lerczak, J. A., Geyer, W. R., & Chant, R. J. (2006). Mechanisms driving the time-dependent salt flux in a partially stratified estuary. *Journal of Physical Oceanography*, *36*(12), 2296–2311. https://doi.org/10.1175/JPO2959.1

Lin, Z., Zhang, H., Lin, H., & Gong, W. (2019). Intraseasonal and interannual variabilities of saltwater intrusion during dry seasons and the associated driving forcings in a partially mixed estuary. *Continental Shelf Research*, *174*, 95–107. https://doi.org/10.1016/j.csr.2019.01.008

Livina, V., Ashkenazy, Y., Kizner, Z., Strygin, V., Bunde, A., & Havlin, S. (2003). A stochastic model of river discharge fluctuations. *Physica A: Statistical Mechanics and its Applications*, *330*(1–2), 283–290. https://doi.org/10.1016/j.physa.2003.08.012

MacCready, P. (1999). Estuarine adjustment to changes in river flow and tidal mixing. *Journal of Physical Oceanography*, *29*(4), 708–726. https://doi.org/10.1175/1520-0485(1999)029<0708:eatcir>2.0.co;2

MacCready, P. (2007). Estuarine adjustment. *Journal of Physical Oceanography*, *37*(8), 2133–2145. https://doi.org/10.1175/JPO3082.1

Martyr-Koller, R., Kernkamp, H., Dam, A. V., Wegen, M. v. d., Lucas, L., Knowles, N., et al. (2017). Application of an unstructured 3D finite volume numerical model to flows and salinity dynamics in the San Francisco bay-delta. *Estuarine, Coastal and Shelf Science*, *192*, 86–107. https://doi.org/10.1016/j.ecss.2017.04.024

Mikosch, T. (2000). *Elementary stochastic calculus*. World Scientific.

Monismith, S. (2016). A note on delta outflow. *San Francisco Estuary and Watershed Science*, *14*(3), 1–16. https://doi.org/10.15447/sfews.2016v14iss3art3

Monismith, S. (2017). An integral model of unsteady salinity intrusion in estuaries. *Journal of Hydraulic Research*, *55*(3), 392–408. https://doi.org/10.1080/00221686.2016.1274682

Monismith, S., Kimmerer, W., Burau, J., & Stacey, M. (2002). Structure and flow-induced variability of the subtidal salinity field in northern San Francisco Bay. *Journal of Physical Oceanography*, *32*(11), 3003–3019. https://doi.org/10.1175/1520-0485(2002)032<3003:safivo>2.0.co;2

Oksendal, B. (1995). *Stochastic differential equations*. Springer-Verlag.

Reyes-Merlo, M. A., Díez-Minguito, M., Ortega-Sánchez, M., Baquerizo, A., & Losada, M. A. (2013). On the relative influence of climate forcing agents on the saline intrusion in a well-mixed estuary: Medium-term Monte Carlo predictions. *Journal of Coastal Research*, *65*, 1200–1205. https://doi.org/10.2112/SI65-203.1

Sapsis, T. P., & Lermusiaux, P. F. J. (2009). Dynamically orthogonal field equations for continuous stochastic dynamical systems. *Physica D*, *238*, 2347–2360. https://doi.org/10.1016/j.physd.2009.09.017

Savenije, H. H. (2005). Salt intrusion in alluvial estuaries. In H. H. Savenije (Ed.), *Salinity and tides in alluvial estuaries* (pp. 137–184). Elsevier Science Ltd. https://doi.org/10.1016/B978-044452107-1/50006-X

Simpson, J., Vennell, R., & Souza, A. (2001). The salt fluxes in a tidally-energetic estuary. *Estuarine, Coastal and Shelf Science*, *52*(1), 131–142. https://doi.org/10.1006/ecss.2000.0733

Sura, P., Fraedrich, K., & Lunkeit, F. (2001). Regime transitions in a stochastically forced double-gyre model. *Journal of Physical Oceanography*, *31*(2), 411–426. https://doi.org/10.1175/1520-0485(2001)031<0411:rtiasf>2.0.co;2

Tian, R. (2019). Factors controlling saltwater intrusion across multi-time scales in estuaries, Chester river, Chesapeake Bay. *Estuarine, Coastal and Shelf Science*, *223*, 61–73. https://doi.org/10.1016/j.ecss.2019.04.041